

First measurements of J/ψ decays into $\Sigma^+\bar{\Sigma}^-$ and $\Xi^0\bar{\Xi}^0$

M. Ablikim¹, J. Z. Bai¹, Y. Bai¹, Y. Ban¹¹, X. Cai¹, H. F. Chen¹⁶, H. S. Chen¹,
H. X. Chen¹, J. C. Chen¹, Jin Chen¹, X. D. Chen⁵, Y. B. Chen¹, Y. P. Chu¹,
Y. S. Dai¹⁸, Z. Y. Deng¹, S. X. Du¹, J. Fang¹, C. D. Fu¹⁴, C. S. Gao¹, Y. N. Gao¹⁴,
S. D. Gu¹, Y. T. Gu⁴, Y. N. Guo¹, Z. J. Guo^{15a}, F. A. Harris¹⁵, K. L. He¹, M. He¹²,
Y. K. Heng¹, J. Hou¹⁰, H. M. Hu¹, T. Hu¹, G. S. Huang^{1b}, X. T. Huang¹², Y. P. Huang¹,
X. B. Ji¹, X. S. Jiang¹, J. B. Jiao¹², D. P. Jin¹, S. Jin¹, Y. F. Lai¹, H. B. Li¹, J. Li¹,
R. Y. Li¹, W. D. Li¹, W. G. Li¹, X. L. Li¹, X. N. Li¹, X. Q. Li¹⁰, Y. F. Liang¹³,
H. B. Liao^{1c}, B. J. Liu¹, C. X. Liu¹, Fang Liu¹, Feng Liu⁶, H. H. Liu^{1d}, H. M. Liu¹,
J. B. Liu^{1e}, J. P. Liu¹⁷, H. B. Liu⁴, J. Liu¹, Q. Liu¹⁵, R. G. Liu¹, S. Liu⁸, Z. A. Liu¹,
F. Lu¹, G. R. Lu⁵, J. G. Lu¹, C. L. Luo⁹, F. C. Ma⁸, H. L. Ma², L. L. Ma^{1f}, Q. M. Ma¹,
M. Q. A. Malik¹, Z. P. Mao¹, X. H. Mo¹, J. Nie¹, S. L. Olsen¹⁵, R. G. Ping¹, N. D. Qi¹,
H. Qin¹, J. F. Qiu¹, G. Rong¹, X. D. Ruan⁴, L. Y. Shan¹, L. Shang¹, C. P. Shen¹⁵,
D. L. Shen¹, X. Y. Shen¹, H. Y. Sheng¹, H. S. Sun¹, S. S. Sun¹, Y. Z. Sun¹, Z. J. Sun¹,
X. Tang¹, J. P. Tian¹⁴, G. L. Tong¹, G. S. Varner¹⁵, X. Wan¹, L. Wang¹, L. L. Wang¹,
L. S. Wang¹, P. Wang¹, P. L. Wang¹, W. F. Wang^{1g}, Y. F. Wang¹, Z. Wang¹,
Z. Y. Wang¹, C. L. Wei¹, D. H. Wei³, Y. Weng¹, N. Wu¹, X. M. Xia¹, X. X. Xie¹,
G. F. Xu¹, X. P. Xu⁶, Y. Xu¹⁰, M. L. Yan¹⁶, H. X. Yang¹, M. Yang¹, Y. X. Yang³,
M. H. Ye², Y. X. Ye¹⁶, C. X. Yu¹⁰, G. W. Yu¹, C. Z. Yuan¹, Y. Yuan¹, S. L. Zang^{1h},
Y. Zeng⁷, B. X. Zhang¹, B. Y. Zhang¹, C. C. Zhang¹, D. H. Zhang¹, H. Q. Zhang¹,
H. Y. Zhang¹, J. W. Zhang¹, J. Y. Zhang¹, X. Y. Zhang¹², Y. Y. Zhang¹³, Z. X. Zhang¹¹,
Z. P. Zhang¹⁶, D. X. Zhao¹, J. W. Zhao¹, M. G. Zhao¹, P. P. Zhao¹, Z. G. Zhao¹ⁱ,
H. Q. Zheng¹¹, J. P. Zheng¹, Z. P. Zheng¹, B. Zhong⁹, L. Zhou¹, K. J. Zhu¹, Q. M. Zhu¹,
X. W. Zhu¹, Y. C. Zhu¹, Y. S. Zhu¹, Z. A. Zhu¹, Z. L. Zhu³, B. A. Zhuang¹, B. S. Zou¹

(BES Collaboration)

¹ *Institute of High Energy Physics, Beijing 100049, People's Republic of China*

² *China Center for Advanced Science and Technology (CCAST),*

Beijing 100080, People's Republic of China

³ *Guangxi Normal University, Guilin 541004, People's Republic of China*

- ⁴ *Guangxi University, Nanning 530004, People's Republic of China*
- ⁵ *Henan Normal University, Xinxiang 453002, People's Republic of China*
- ⁶ *Huazhong Normal University, Wuhan 430079, People's Republic of China*
- ⁷ *Hunan University, Changsha 410082, People's Republic of China*
- ⁸ *Liaoning University, Shenyang 110036, People's Republic of China*
- ⁹ *Nanjing Normal University, Nanjing 210097, People's Republic of China*
- ¹⁰ *Nankai University, Tianjin 300071, People's Republic of China*
- ¹¹ *Peking University, Beijing 100871, People's Republic of China*
- ¹² *Shandong University, Jinan 250100, People's Republic of China*
- ¹³ *Sichuan University, Chengdu 610064, People's Republic of China*
- ¹⁴ *Tsinghua University, Beijing 100084, People's Republic of China*
- ¹⁵ *University of Hawaii, Honolulu, HI 96822, USA*
- ¹⁶ *University of Science and Technology of
China, Hefei 230026, People's Republic of China*
- ¹⁷ *Wuhan University, Wuhan 430072, People's Republic of China*
- ¹⁸ *Zhejiang University, Hangzhou 310028, People's Republic of China*
- ^a *Current address: Johns Hopkins University, Baltimore, MD 21218, USA*
- ^b *Current address: University of Oklahoma, Norman, Oklahoma 73019, USA*
- ^c *Current address: DAPNIA/SPP Batiment 141,
CEA Saclay, 91191, Gif sur Yvette Cedex, France*
- ^d *Current address: Henan University of Science and
Technology, Luoyang 471003, People's Republic of China*
- ^e *Current address: CERN, CH-1211 Geneva 23, Switzerland*
- ^f *Current address: University of Toronto, Toronto M5S 1A7, Canada*
- ^g *Current address: Laboratoire de l'Accélérateur Linéaire, Orsay, F-91898, France*
- ^h *Current address: University of Colorado, Boulder, CO 80309, USA*
- ⁱ *Current address: University of Michigan, Ann Arbor, MI 48109, USA*

(Dated: October 27, 2018)

Abstract

Based on 58 million J/ψ events collected with the BESII detector at the BEPC, the baryon pair processes $J/\psi \rightarrow \Sigma^+\bar{\Sigma}^-$ and $J/\psi \rightarrow \Xi^0\bar{\Xi}^0$ are observed for the first time. The branching fractions are measured to be $\mathcal{B}(J/\psi \rightarrow \Sigma^+\bar{\Sigma}^-) = (1.50 \pm 0.10 \pm 0.22) \times 10^{-3}$ and $\mathcal{B}(J/\psi \rightarrow \Xi^0\bar{\Xi}^0) = (1.20 \pm 0.12 \pm 0.21) \times 10^{-3}$, where the first errors are statistical and the second ones are systematic.

PACS numbers: 13.25.Gv, 12.38.Qk, 14.20.Gk, 14.40.Cs

I. INTRODUCTION

Since the discovery of the charmonium states J/ψ and $\psi(2S)$, a number of baryonic decay channels have been studied by several different experiments [1, 2, 3, 4, 5, 6, 7, 8, 9, 10, 11, 12]. Baryon-antibaryon decays, which provide a test of the predictive power of QCD, have especially attracted interest of both theoretical and experimental experts. Among these decays, $J/\psi \rightarrow \Sigma^0 \bar{\Sigma}^0$ and $J/\psi \rightarrow \Xi^- \bar{\Xi}^+$ have been studied by DM2 and MarkII [2, 3], but their isospin partners decays $J/\psi \rightarrow \Sigma^+ \bar{\Sigma}^-$ and $J/\psi \rightarrow \Xi^0 \bar{\Xi}^0$ have not been measured before. In this article, we study $J/\psi \rightarrow \Sigma^+ \bar{\Sigma}^-$ and $J/\psi \rightarrow \Xi^0 \bar{\Xi}^0$ using the large J/ψ data sample accumulated with the BESII detector. The decay mode $J/\psi \rightarrow \Sigma^- \bar{\Sigma}^+$ is not studied here since the final states contain a neutron and an antineutron, which are difficult to detect with the BESII detector. Isospin invariance predicts $\mathcal{B}(\Sigma^+ \bar{\Sigma}^-) = \mathcal{B}(\Sigma^0 \bar{\Sigma}^0)$ and $\mathcal{B}(\Xi^0 \bar{\Xi}^0) = \mathcal{B}(\Xi^- \bar{\Xi}^+)$. However in the quark model, there are well-known isospin breaking contributions in J/ψ baryonic decays [13, 14].

II. THE BESII DETECTOR AND MONTE CARLO SIMULATION

BESII is a conventional solenoidal magnet detector that is described in detail in Ref. [15]. A 12-layer vertex chamber (VTC) surrounding the beam pipe provides trigger and track information. A forty-layer main drift chamber (MDC), located radially outside the VTC, provides trajectory and energy loss (dE/dx) information for charged tracks over 85% of the total solid angle. The momentum resolution is $\sigma_p/p = 0.017\sqrt{1+p^2}$ (p in GeV/ c), and the dE/dx resolution for hadron tracks is $\sim 8\%$. An array of 48 scintillation counters surrounding the MDC measures the time-of-flight (TOF) of charged tracks with a resolution of ~ 200 ps for hadrons. Radially outside the TOF system is a 12 radiation length, lead-gas barrel shower counter (BSC). This measures the energies of electrons and photons over $\sim 80\%$ of the total solid angle with an energy resolution of $\sigma_E/E = 22\%/\sqrt{E}$ (E in GeV). Outside of the solenoidal coil, which provides a 0.4 Tesla magnetic field over the tracking volume, is an iron flux return that is instrumented with three double layers of counters that identify muons of momentum greater than 0.5 GeV/ c .

In this analysis, a GEANT3 based Monte Carlo (MC) simulation program [16] with

detailed consideration of real detector responses (such as dead electronic channels) is used. The consistency between data and MC simulation has been carefully checked in many high-purity physics channels, and the agreement is quite reasonable [17].

III. EVENT SELECTION

The data sample used for this analysis consists of $(58.0 \pm 2.7) \times 10^6$ J/ψ events collected with the BESII detector [18]. The decay channels investigated are J/ψ decays into $\Sigma^+\bar{\Sigma}^-$ and $\Xi^0\bar{\Xi}^0$ baryon pairs, where Σ^+ decays to $\pi^0 p$ ($\pi^0 \rightarrow \gamma\gamma$), Ξ^0 to $\pi^0\Lambda$ ($\Lambda \rightarrow \pi^- p$). Therefore the final states for the two decays are $p\bar{p}\gamma\gamma\gamma\gamma$ and $\pi^+\pi^-p\bar{p}\gamma\gamma\gamma\gamma$, respectively. Both decays contain four photons in the final states. Candidate events are required to satisfy the following common selection criteria:

1. Events must have two or four good charged tracks with zero net charge. A good charged track is a track that is well fitted to a helix in the MDC, and has a polar angle, θ , in the range $|\cos\theta| < 0.8$. For $J/\psi \rightarrow \Sigma^+\bar{\Sigma}^-$, tracks are required to originate from the interaction region of $R_{xy} < 0.02$ m and $|z| < 0.2$ m, where R_{xy} is the distance from the beamline to the point of closest approach of the track to the beamline, and $|z|$ is the distance along the beamline to this point from the interaction point. For $J/\psi \rightarrow \Xi^0\bar{\Xi}^0$, because of the long lifetime of Ξ and Λ , tracks are not required to originate from the interaction region.
2. The TOF and dE/dx measurements of the charged tracks are used to calculate χ_{PID}^2 values for the hypotheses that the particle is a pion, kaon, or proton. Only the two proton tracks must be identified with the requirement that χ_{PID}^2 for the proton hypothesis is less than those for the π or K hypotheses.
3. Isolated photons are those that have energy deposited in the BSC greater than 50 MeV, and the angle between the photon entering the BSC and the shower development direction in the BSC is less than 37° . In order to remove the fake photons produced by \bar{p} annihilation and those produced by hadronic interactions of tracks, the angle between the photon and antiproton is required to be larger than 25° and those between the photon and other charged tracks larger than 8° .

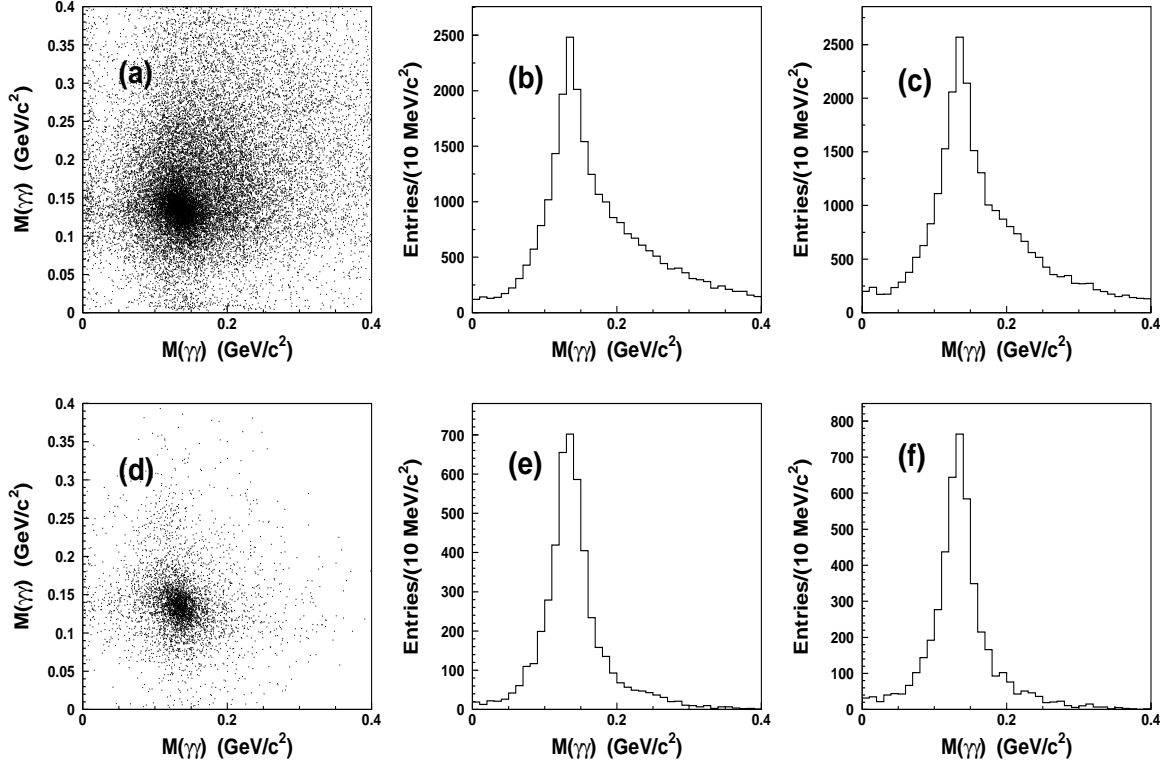


FIG. 1: Invariant mass distributions of two photons for $J/\psi \rightarrow \Sigma^+ \bar{\Sigma}^-$ candidate events. (a) Scatter plot of $M(\gamma\gamma)_1$ versus $M(\gamma\gamma)_2$ for the combination with the minimum $R(\pi^0)$, (b) distribution of $M(\gamma\gamma)_1$, (c) distribution of $M(\gamma\gamma)_2$ in the data sample. and (d), (e), and (f) are the corresponding plots for MC simulated $J/\psi \rightarrow \Sigma^+ \bar{\Sigma}^-$ events.

Different kinematic fits are used in the selection of the two decay channels. A four constraint (4C) kinematic fit under the $p\bar{p}\gamma\gamma\gamma\gamma$ hypothesis is performed for $J/\psi \rightarrow \Sigma^+ \bar{\Sigma}^-$. If there are more than four photon candidates in an event, all combinations are tried, and the combination with the smallest χ_{4C}^2 is retained. We require the minimum χ_{4C}^2 to be less than 15. For $J/\psi \rightarrow \Xi^0 \bar{\Xi}^0$, a six constraint (6C) kinematic fit under the hypothesis $J/\psi \rightarrow \gamma\gamma\gamma\gamma\pi^+\pi^-p\bar{p}$ with the invariant mass of the two photon pairs constrained to the π^0 mass is performed, and the χ^2 of the 6C fit is required to be less than 50.

IV. DATA ANALYSIS

A. $J/\psi \rightarrow \Sigma^+ \bar{\Sigma}^-$

The candidate events for this decay mode contain two π^0 , and there are three possible combinations of $(\gamma\gamma)_1$ $(\gamma\gamma)_2$ to form a π^0 pair. The π^0 pair with the minimum $R(\pi^0)$, where $R(\pi^0) = \sqrt{(M(\gamma\gamma)_1 - M(\pi^0))^2 + (M(\gamma\gamma)_2 - M(\pi^0))^2}$, is chosen for further analysis. Figure 1 shows the mass distributions of candidate events with the minimum $R(\pi^0)$ for data and MC samples, respectively. A clear $\pi^0\pi^0$ signal is observed in the data sample. In order to select π^0 pair events, $|M(\gamma\gamma)_1 - M(\pi^0)| < 0.03 \text{ GeV}/c^2$ and $|M(\gamma\gamma)_2 - M(\pi^0)| < 0.03 \text{ GeV}/c^2$ are required.

After π^0 selection, there are still two possible $\pi^0 p$ combinations from which to form the Σ of the $\Sigma^+ \bar{\Sigma}^-$ pair. The combination having the smallest value of $R(\Sigma) = \sqrt{(M(\pi_{(1)}^0 p) - M(\Sigma))^2 + (M(\pi_{(2)}^0 \bar{p}) - M(\Sigma))^2}$ is selected for further analysis. Figure 2 shows the πp invariant mass for data and MC simulated $J/\psi \rightarrow \Sigma^+ \bar{\Sigma}^-$ events. A clear $\Sigma^+ \bar{\Sigma}^-$ signal is seen in the bottom left corner of Fig. 2(a). Figure 2(b) is the $M(\pi_{(1)}^0 p)$ distribution by requiring $|M(\pi_{(2)}^0 \bar{p}) - M(\Sigma)| < 0.03 \text{ GeV}/c^2$, (c) is the $M(\pi_{(2)}^0 \bar{p})$ distribution by requiring $|M(\pi_{(1)}^0 p) - M(\Sigma)| < 0.03 \text{ GeV}/c^2$, and (d) is the sum of (b) and (c) scaled by a factor of 0.5.

Possible backgrounds come from channels with $p\bar{p}$ production, including $J/\psi \rightarrow p\bar{p}$, $J/\psi \rightarrow \gamma p\bar{p}$, $J/\psi \rightarrow p\bar{p}\pi^0$, $J/\psi \rightarrow p\bar{p}\eta$ ($\eta \rightarrow \gamma\gamma$ or $\eta \rightarrow 3\pi^0$), $J/\psi \rightarrow p\bar{p}\omega$ ($\omega \rightarrow \gamma\pi^0$), and $J/\psi \rightarrow p\bar{p}\pi^0\pi^0$. MC events are generated with a phase space generator for the first two background channels. None or only a few events survive the selection criteria; therefore contamination from the first two channels is negligible. For $J/\psi \rightarrow p\bar{p}\pi^0$, $J/\psi \rightarrow p\bar{p}\eta$, and $J/\psi \rightarrow p\bar{p}\omega$, MC events are also generated according to phase space. Using the branching fractions from the PDG [19], the numbers of events from these channels are expected to be 7.2, 72.4 and 7.8 in the whole πp mass region, respectively. For $J/\psi \rightarrow p\bar{p}\pi^0\pi^0$, the branching fraction is unavailable, so the normalized number of events for this background can not be determined. However, the πp invariant mass distribution from all backgrounds is smooth, so these backgrounds will not affect the determination of the number of signal events in fitting the πp mass distribution.

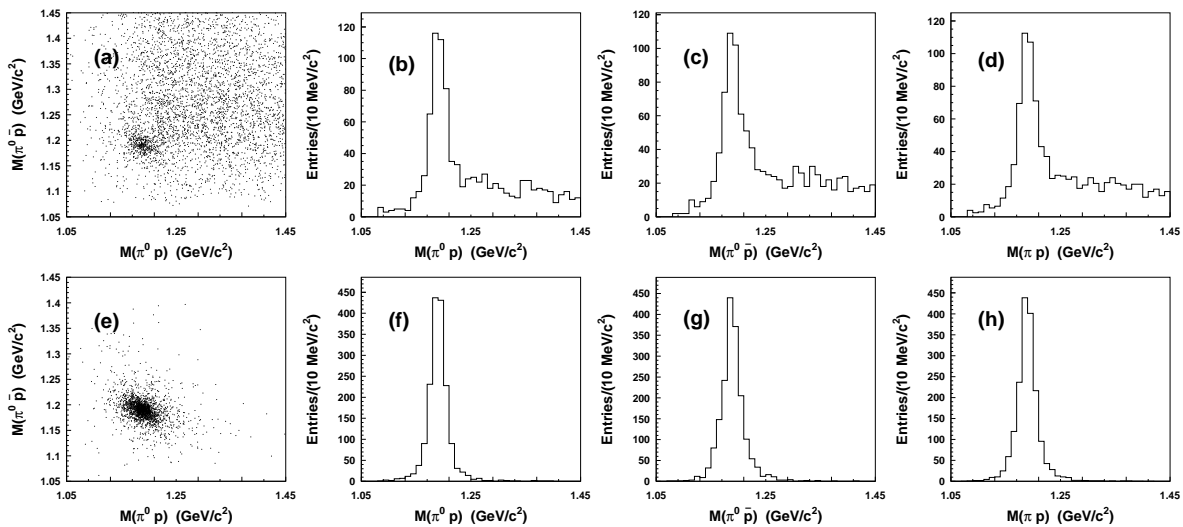


FIG. 2: Distributions for $J/\psi \rightarrow \Sigma^+\bar{\Sigma}^-$ candidate events. (a) Scatter plot of $M(\pi_{(1)}^0 p)$ versus $M(\pi_{(2)}^0 \bar{p})$; (b) $M(\pi_{(1)}^0 p)$ distribution by requiring $|M(\pi_{(2)}^0 \bar{p}) - M(\Sigma^+)| < 0.03 \text{ GeV}/c^2$, (c) $M(\pi_{(2)}^0 \bar{p})$ distribution by requiring $|M(\pi_{(1)}^0 p) - M(\Sigma^+)| < 0.03 \text{ GeV}/c^2$, and (d) is the sum of (b) and (c) scaled by a factor of 0.5. (e), (f), (g) and (h) are the corresponding plots of (a), (b), (c) and (d) for MC simulated $J/\psi \rightarrow \Sigma^+\bar{\Sigma}^-$ events.

In order to determine the branching fraction, we fit the Σ signal in Fig. 2(d) with a histogram of the signal shape from MC simulation together with a second order polynomial for the background. The fit is shown in Fig. 3, and it yields 399 ± 26 signal events, with the goodness of the fit being $\chi^2/ndf = 22.4/31 \approx 0.72$. The $J/\psi \rightarrow \Sigma^+\bar{\Sigma}^-$ efficiency is determined to be $\varepsilon=1.75\%$ using MC simulated signal events, and the branching fraction is,

$$\begin{aligned} \mathcal{B}(J/\psi \rightarrow \Sigma^+\bar{\Sigma}^-) &= \frac{N(\Sigma)/\varepsilon}{N(J/\psi) \cdot \mathcal{B}^2(\Sigma^+ \rightarrow \pi^0 p) \cdot \mathcal{B}^2(\pi^0 \rightarrow \gamma\gamma)} \\ &= (1.50 \pm 0.10) \times 10^{-3}, \end{aligned}$$

where the error is statistical.

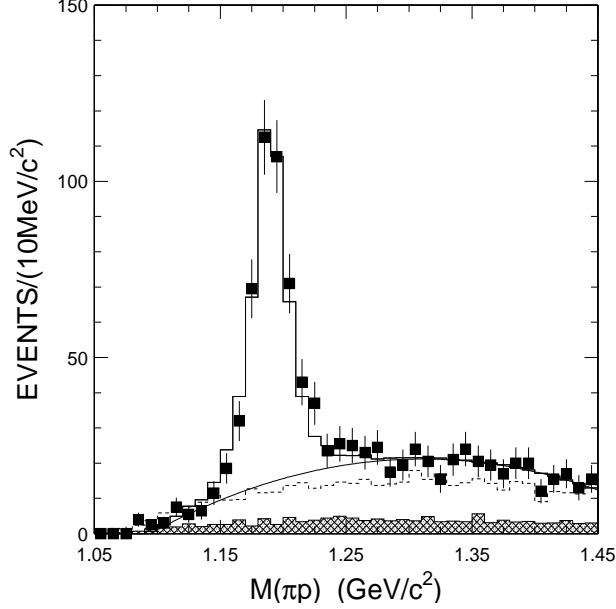


FIG. 3: Fit to πp invariant mass of $J/\psi \rightarrow \Sigma^+ \bar{\Sigma}^-$ candidate events with MC simulated signal shape and a second order polynomial as background shape. The shaded histogram is background from MC simulated $J/\psi \rightarrow p\bar{p}\pi^0$, $J/\psi \rightarrow p\bar{p}\eta$, and $J/\psi \rightarrow p\bar{p}\omega$, normalized according to the branching fractions in PDG [19]. The dashed histogram shows the shape of MC simulated $J/\psi \rightarrow p\bar{p}\pi^0\pi^0$ normalized using an assigned branching fraction of 0.003.

B. $J/\psi \rightarrow \Xi^0 \bar{\Xi}^0$

The candidate events for this decay mode contain a $\Lambda \bar{\Lambda}$ pair. In order to select $\Lambda \bar{\Lambda}$ events, we require the $\pi^- p$ and $\pi^+ \bar{p}$ invariant masses satisfy $|M(\pi^- p) - M(\Lambda)| < 0.01 \text{ GeV}/c^2$ and $|M(\pi^+ \bar{p}) - M(\Lambda)| < 0.01 \text{ GeV}/c^2$.

There are three possible combinations of the four photons to form a π^0 pair in the 6C kinematic fit; the combination with the minimum χ_{6C}^2 is considered to be the correct one and selected for further investigation. After π^0 pairs are selected, there are two possible combinations $(\pi_{(1)}^0 \Lambda, \pi_{(2)}^0 \bar{\Lambda})$ to form Ξ^0 candidates. Analogous to the analysis of $\Sigma^+ \bar{\Sigma}^-$, we choose the combination with the lowest value of $R(\Xi^0) = \sqrt{(M(\pi_{(1)}^0 \Lambda) - M(\Xi^0))^2 + (M(\pi_{(2)}^0 \bar{\Lambda}) - M(\Xi^0))^2}$ for further study. Figure 4 shows the $\pi \Lambda$ invariant mass for this case for data and MC simulated $J/\psi \rightarrow \Xi^0 \bar{\Xi}^0$ events. In Fig. 4 (a), besides the clear $\Xi^0 \bar{\Xi}^0$, $\Sigma(1385)^0 \bar{\Sigma}(1385)^0$ production is also visible. In Fig. 4 (b) is

the $M(\pi_{(1)}^0 \Lambda)$ distribution after requiring $|M(\pi_{(2)}^0 \bar{\Lambda}) - M(\Xi^0)| < 0.03 \text{ GeV}/c^2$, (c) is the $M(\pi_{(2)}^0 \bar{\Lambda})$ distribution requiring $|M(\pi_{(1)}^0 \Lambda) - M(\Xi^0)| < 0.03 \text{ GeV}/c^2$, and (d) is the sum of (b) and (c) scaled by a factor of 0.5.

Possible backgrounds come from channels with Λ or Ξ production, including $J/\psi \rightarrow \Sigma^0 \bar{\Sigma}^0$, $J/\psi \rightarrow \Sigma^0 \pi^0 \bar{\Lambda} (+c.c.)$, $J/\psi \rightarrow \Sigma(1385)^0 \bar{\Sigma}(1385)^0$, and $J/\psi \rightarrow \pi^0 \pi^0 \Lambda \bar{\Lambda}$. Using the branching fraction of $J/\psi \rightarrow \Sigma^0 \bar{\Sigma}^0$ from the PDG [19] and assuming isospin invariance holds for $J/\psi \rightarrow \Sigma \pi \bar{\Lambda} + c.c.$ and $J/\psi \rightarrow \Sigma(1385) \bar{\Sigma}(1385)$, we obtain 0.6, 45.9, and 51.3 background events from MC simulation, respectively. The shaded part in Fig. 5 shows the normalized simulated backgrounds from the first three channels, which do not exhibit any peaking structures in the Ξ^0 mass region. Since the branching fraction is unavailable for $J/\psi \rightarrow \pi^0 \pi^0 \Lambda \bar{\Lambda}$, we do not determine the normalized number of events for this decay mode. However, MC simulation indicates that the $\pi \Lambda$ invariant mass distribution is

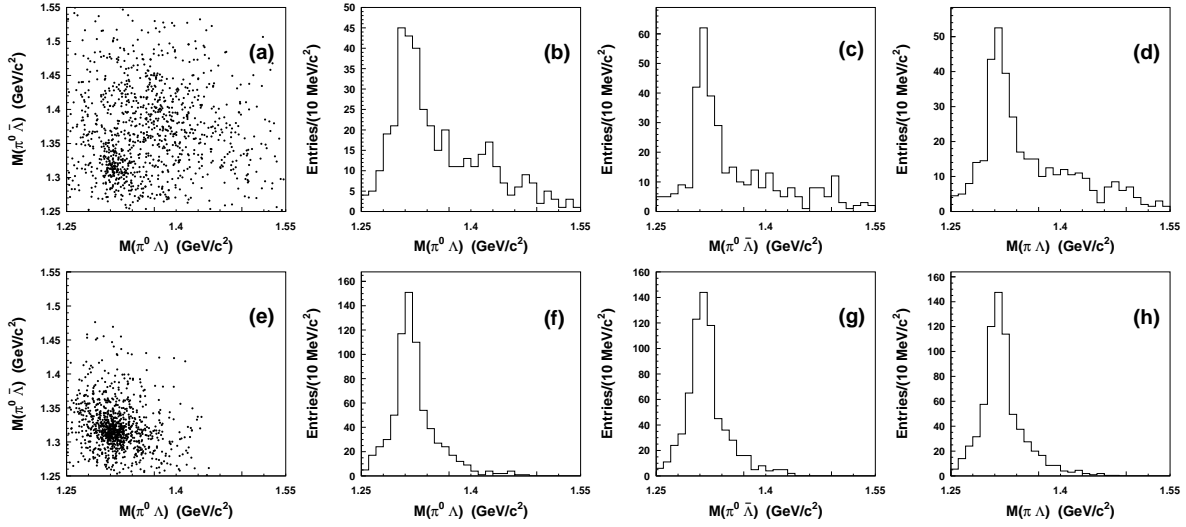


FIG. 4: Plots for $J/\psi \rightarrow \Xi^0 \bar{\Xi}^0$ candidate events. (a) is the scatter plot of $M(\pi_{(1)}^0 \Lambda)$ versus $M(\pi_{(2)}^0 \bar{\Lambda})$, (b) is the $M(\pi_{(1)}^0 \Lambda)$ distribution recoiling against $\bar{\Xi}^0$, selected by requiring $|M(\pi_{(2)}^0 \bar{\Lambda}) - M(\Xi^0)| < 0.03 \text{ GeV}/c^2$, (c) is the $M(\pi_{(2)}^0 \bar{\Lambda})$ distribution recoiling against Ξ^0 , selected by requiring $|M(\pi_{(1)}^0 \Lambda) - M(\Xi^0)| < 0.03 \text{ GeV}/c^2$, (d) is the sum of (b) and (c) scaled by a factor of 0.5, (e), (f), (g) and (h) are the corresponding plots of (a), (b), (c), and (d) for MC simulated $J/\psi \rightarrow \Xi^0 \bar{\Xi}^0$ events.

smooth without any peaking, and therefore this background will not affect the determination of the number of signal events. We also studied backgrounds from $\Lambda\bar{\Lambda}$ sidebands and other possible background channels listed in the PDG, but the contaminations were found to be negligible. The fitted number of signal events is insensitive to the shape of all the backgrounds considered here. The numbers of signal events using different background shapes differ slightly from each other; we consider this difference as one source of systematic error.

To get the number of signal events, we fit the observed Ξ signal in Fig. 4 (d) by a histogram of the signal shape from MC simulation plus a second order polynomial as the background. The fitting result is shown in Fig. 5 and the fit yields 206 ± 20 . The efficiency is determined to be $\varepsilon=0.74\%$ using MC simulated signal events generated according to a phase space distribution. The branching fraction is,

$$\begin{aligned} \mathcal{B}(J/\psi \rightarrow \Xi^0 \bar{\Xi}^0) &= \frac{N(\Xi)/\varepsilon}{N(J/\psi) \cdot \mathcal{B}^2(\Xi^0 \rightarrow \pi^0 \Lambda) \cdot \mathcal{B}^2(\Lambda \rightarrow \pi^- p) \cdot \mathcal{B}^2(\pi^0 \rightarrow \gamma\gamma)} \\ &= (1.20 \pm 0.12) \times 10^{-3}, \end{aligned}$$

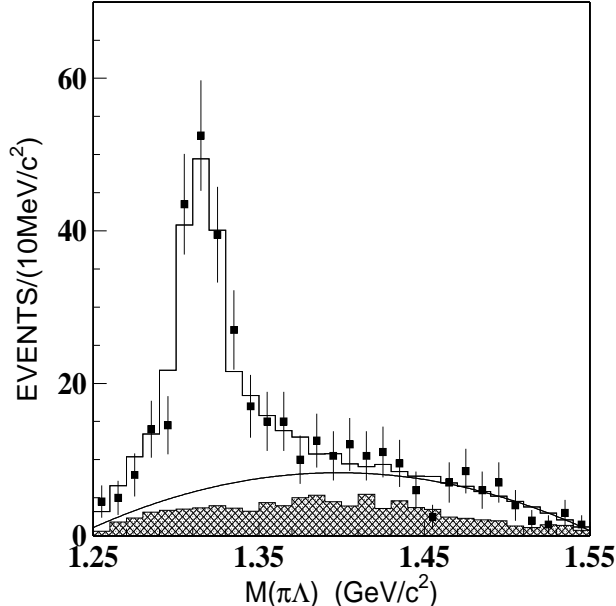


FIG. 5: Fit to $\pi\Lambda$ invariant mass spectrum of $J/\psi \rightarrow \Xi^0 \bar{\Xi}^0$ candidate events. Dots with error bars are data, the hatched histogram is the normalized background from all the channels considered in the text, and the solid histogram is the fit to data using a histogram of the signal shape from MC simulation plus a second order polynomial for background.

where the error is statistical.

V. SYSTEMATIC ERRORS

The systematic errors on the branching ratios mainly arise from the uncertainties in the MDC tracking, particle identification, photon efficiency, angular distribution parameter α in event generators, kinematic fitting, background shapes, and the total number of J/ψ events. The errors from different sources are listed in Table I.

The uncertainties caused by MDC tracking and particle identification (PID) are estimated by the difference of the selection efficiency of proton and antiproton between data and MC simulation [20]. The efficiencies of PID and track reconstruction for protons and antiprotons that enter the detector being reconstructed and identified are measured using samples of $J/\psi \rightarrow \pi^+\pi^-p\bar{p}$, which are selected using PID for three tracks, allowing one proton or antiproton at a time to be missing in the fit [20]. It is found that the efficiency difference of one proton identification is about 1% for $J/\psi \rightarrow \Sigma^+\bar{\Sigma}^-$ and about 2% for $J/\psi \rightarrow \Xi^0\bar{\Xi}^0$ depending on the momentum of the final state particles. The π^\pm tracking and PID efficiencies are simulated within 1% per track. Therefore we get a total of 2% for $J/\psi \rightarrow \Sigma^+\bar{\Sigma}^-$ and 6% for $J/\psi \rightarrow \Xi^0\bar{\Xi}^0$, respectively.

TABLE I: Summary of systematic errors (%).

Source	$J/\psi \rightarrow \Sigma^+\bar{\Sigma}^-$	$J/\psi \rightarrow \Xi^0\bar{\Xi}^0$
MDC tracking and PID	2	6
Photon efficiency	8	8
Kinematic fit	4	8.4
Background shape	6	5
J/ψ statistics	4.7	4.7
α	8	7
VC trigger efficiency	1	4
Total	14.4	16.9

The photon detection efficiency is studied using $J/\psi \rightarrow \rho^0\pi^0$ in Ref. [21]. The results indicate that the systematic error is about 2% for each photon. Therefore, 8% is taken as the systematic error of photon efficiency for the two decay modes.

The angular distribution of the baryon in J/ψ decay is $1 + \alpha \cos^2 \theta$, with θ being the polar angle of the baryon in J/ψ rest frame. To estimate the uncertainty originating from the angular distribution parameter α , we generate MC samples for $\alpha = 0$ and $\alpha = 1$, separately. The differences of efficiency between $\alpha = 0$ and $\alpha = 1$ are taken as systematic errors, which is 8% for $J/\psi \rightarrow \Sigma^+\bar{\Sigma}^-$ and 7% for $J/\psi \rightarrow \Xi^0\bar{\Xi}^0$.

The systematic errors for the kinematic fits are 4% for $\Sigma^+\bar{\Sigma}^-$ and 8.4% for $\Xi^0\bar{\Xi}^0$, they are taken from earlier studies [22, 23]. The VTC trigger efficiency systematic errors are estimated to be 1% for $\Sigma^+\bar{\Sigma}^-$ and 4% for $\Xi^0\bar{\Xi}^0$.

The systematic error of the background shape used is estimated by measuring the difference of the numbers of fitted signal events for different background shapes. For $J/\psi \rightarrow \Sigma^+\bar{\Sigma}^-$, we also fit the πp invariant mass distribution using the normalized background, or MC simulated $J/\psi \rightarrow \pi^0\pi^0 p\bar{p}$ events as the background shape. The difference of the numbers of signal events is about 6% compared to our nominal fit, which is taken as the systematic error of the background shape. For $J/\psi \rightarrow \Xi^0\bar{\Xi}^0$, we fit the $\pi\Lambda$ invariant mass distribution using the normalized background or MC simulated $J/\psi \rightarrow \pi^0\pi^0\Lambda\bar{\Lambda}$ events as the background shape, and we estimate a systematic error of about 5%.

Uncertainty on the total number of J/ψ events is 4.7% [18]. Combining these errors in quadrature gives total systematic errors of 14.4% for $J/\psi \rightarrow \Sigma^+\bar{\Sigma}^-$ and 16.9% for $J/\psi \rightarrow \Xi^0\bar{\Xi}^0$.

VI. RESULTS AND DISCUSSION

Based on $58 \times 10^6 J/\psi$ events accumulated at BESII, we report first measurements of the branching fractions of J/ψ decays into the baryon pairs $\Sigma^+\bar{\Sigma}^-$ and $\Xi^0\bar{\Xi}^0$. The results are listed in Table II, including the results of $J/\psi \rightarrow \Sigma^0\bar{\Sigma}^0$ and $J/\psi \rightarrow \Xi^-\bar{\Xi}^+$. We note that the isospin partners, Σ^+ and Σ^0 and also Ξ^0 and Ξ^- , have similar branching fractions in agreement with expectations of isospin symmetry. Furthermore, according to the phase

space corrected branching fraction $|M_i|^2 = \mathcal{B}(J/\psi \rightarrow B_i \bar{B}_i)/(\pi p^*/\sqrt{s})$ [5], we obtain the phase space corrected branching fractions $(1.50 \pm 0.10 \pm 0.22)$ and $(1.45 \pm 0.15 \pm 0.26)$ for $J/\psi \rightarrow \Sigma^+ \bar{\Sigma}^-$ and $J/\psi \rightarrow \Xi^0 \bar{\Xi}^0$, respectively. We note that the increase of strangeness does not greatly change the branching fraction, indicating the flavor symmetric nature of gluons. We also calculate the ratios of the $\psi(2S)$ results in Ref. [6] to those from J/ψ measurements in this article after removing the phase space factor, and obtain $(14.3 \pm 5.2)\%$ for $\Sigma^+ \bar{\Sigma}^-$ and $(17.3 \pm 6.7)\%$ for $\Xi^0 \bar{\Xi}^0$. They agree with the so called "12% rule" predicted by perturbative QCD [24] within 1σ .

VII. ACKNOWLEDGMENTS

The BES collaboration thanks the staff of BEPC and computing center for their hard efforts. This work is supported in part by the National Natural Science Foundation of China under contracts Nos. 10491300, 10825524, 10225524, 10225525, 10425523, 10625524, 10521003, the Chinese Academy of Sciences under contract No. KJ 95T-03, the 100 Talents Program of CAS under Contract Nos. U-11, U-24, U-25, and the Knowledge Innovation Project of CAS under Contract Nos. U-602, U-34 (IHEP), U-612(IHEP), the National Natural Science Foundation of China under Contract Nos. 10225522, 10491305 (Tsinghua University), MOE of China under contract No. IRT0624 (CCNU), and the

TABLE II: Branching fractions (10^{-3}) of J/ψ decays into $\Sigma^+ \bar{\Sigma}^-$, $\Sigma^0 \bar{\Sigma}^0$, $\Xi^0 \bar{\Xi}^0$, and $\Xi^- \bar{\Xi}^+$ [1, 2, 3, 7, 11]. The first error is statistical and the second systematic. For the results of MarkI [1], the statistical and systematic errors were added in quadrature.

Channels	$J/\psi \rightarrow \Sigma^0 \bar{\Sigma}^0$	$J/\psi \rightarrow \Xi^- \bar{\Xi}^+$	$J/\psi \rightarrow \Sigma^+ \bar{\Sigma}^-$	$J/\psi \rightarrow \Xi^0 \bar{\Xi}^0$
MarkI	1.3 ± 0.4	1.4 ± 0.5		$3.2 \pm 0.8(\Xi^0 \bar{\Xi}^0 + \Xi^- \bar{\Xi}^+)$
MarkII	$1.58 \pm 0.16 \pm 0.25$	$1.14 \pm 0.08 \pm 0.20$		
DM2	$1.06 \pm 0.04 \pm 0.23$	$1.4 \pm 0.12 \pm 0.24$		
BESII	$1.33 \pm 0.04 \pm 0.11$		$1.50 \pm 0.10 \pm 0.22$	$1.20 \pm 0.12 \pm 0.21$
BaBar	$1.15 \pm 0.24 \pm 0.03$			

- [1] MarkI Collaboration, I. Peruzzi *et al.*, Phys. Rev. D **17**, 2901 (1978).
- [2] MarkII Collaboration, M. W. Eaton *et al.*, Phys. Rev. D **29**, 804 (1984).
- [3] DM2 Collaboration, P. Henrard *et al.*, Nucl. Phys. B **292**, 653 (1987).
- [4] BES Collaboration, J. Z. Bai *et al.*, Phys. Lett. B **424**, 213 (1998).
- [5] BES Collaboration, J. Z. Bai *et al.*, Phys. Rev. D **63**, 032002 (2001).
- [6] CLEO Collaboration, T. K. Pedlar *et al.*, Phys. Rev. D **72**, 051108 (2005).
- [7] BES Collaboration, M. Ablikim *et al.*, Phys. Lett. B **632**, 181 (2006).
- [8] BES Collaboration, M. Ablikim *et al.*, Phys. Lett. B **648**, 149 (2007).
- [9] DM2 Collaboration, P. Henrard *et al.*, Nucl. Phys. B **292**, 670 (1987).
- [10] BES Collaboration, M. Ablikim *et al.*, Phys. Rev. Lett. **97**, 062001 (2006).
- [11] BABAR Collaboration, B. Aubert *et al.*, Phys. Rev. D **76**, 092006 (2007).
- [12] BES Collaboration, M. Ablikim *et al.*, Phys. Rev. D **76**, 092003 (2007).
- [13] H. Kowalski and T. F. Walsh, Phys. Rev. D **14**, 852 (1976).
- [14] L. Köpke and N. Wermes, Phys. Rep. **174**, 67 (1989).
- [15] BES Collaboration, J. Z. Bai *et al.*, Nucl. Instrum. Meth. A **458**, 627 (2001).
- [16] CERN Application Software Group, GEANT Detector Description and Simulation Tool, CERN Program Library Long Writeup W 5013, Geneva (1994).
- [17] BES Collaboration, M. Ablikim *et al.*, Nucl. Instrum. Meth. A **552**, 344 (2005).
- [18] S.S. Fang *et al.*, HEP&NP **27**, 277 (2003).
- [19] Particle Data Group, C. Amsler *et al.*, Phys. Lett. B **667**, 1 (2008).
- [20] BES Collaboration, M. Ablikim *et al.*, Phys. Rev. D **71**, 072006 (2005).
- [21] BES Collaboration, J. Z. Bai *et al.*, Phys. Rev. D **70**, 012005 (2004).
- [22] BES Collaboration, M. Ablikim *et al.*, Phys. Rev. D **69**, 072001 (2004).
- [23] BES Collaboration, M. Ablikim *et al.*, Phys. Lett. B **630**, 7 (2005).
- [24] MarkII Collaboration, M. E. B. Franklin *et al.*, Phys. Rev. Lett. **51**, 963 (1983).